Observation of spin-wave dark soliton pairs in yttrium iron garnet thin films

Zihui Wang,[1] Mikhail Cherkasskii,[2] Boris A. Kalinikos,[1,2] and Mingzhong Wu[1,*]
[1]*Department of Physics, Colorado State University, Fort Collins, Colorado 80523, USA*
[2]*St. Petersburg Electrotechnical University, 197376 St. Petersburg, Russia*
(Received 25 September 2014; published 18 May 2015)

The formation of a pair of dark solitons from a single nonlinear black spin-wave pulse was observed. The experiments were carried out with a long and narrow magnetic yttrium iron garnet film strip in a surface spin-wave configuration. The black spin-wave pulses were excited by the use of microwave black pulses—large-amplitude microwaves with narrow squarelike dips. Pairs of black solitons were observed in certain input power and input black pulse width ranges. For each pair, the two solitons show opposite π phase jumps and an overall phase change of zero. Beyond those power and width ranges, one also observed pairs of gray solitons that showed opposite phase jumps and a zero total phase change. The formation of a single black soliton was also observed, but only for an input black pulse that was very narrow. The experimental observations were reproduced by numerical simulations based on the complex Ginzburg-Landau equation.

DOI: 10.1103/PhysRevB.91.174418 PACS number(s): 05.45.Yv, 75.30.Ds, 75.50.Gg, 75.70.Ak

Due to dispersion, a narrow dip on a continuous wave broadens as the wave propagates. If the wave amplitude is large, the dip broadening can be further enhanced by the nonlinearity. This is true for waves that have an attractive nonlinearity. For waves with a repulsive nonlinearity, however, the nonlinearity can give rise to a self-narrowing effect that can cancel the dispersion-produced broadening of the dip. When a fine balance is achieved between the two effects, the dip on the continuous wave can evolve into a stable localized excitation—an envelope dark soliton [1–5]. There are two types of dark solitons, *black* and *gray*. When the dip amplitude at the soliton center goes to zero, one has a black soliton. When the amplitude at the dip is nonzero, one has a gray soliton. Both the black and gray solitons have a jump in the carrier wave phase at their centers. For black solitons, such a phase jump is exactly equal to π. For gray solitons, the jump is between 0 and π.

From a physical point of view, a straightforward way to excite a dark envelope soliton is to use a dark input pulse—a narrow dip in the amplitude or intensity of a continuous wave background. This approach has indeed been previously used to excite black envelope solitons, for example, for surface spin waves in magnetic yttrium iron garnet (YIG) thin film strips [6] and for lasers in photorefractive crystals [7]. Theoretically, however, an initial dark signal should not evolve into a single dark soliton. Rather, it should develop into a pair of dark solitons that have opposite phase jumps and an overall phase change of zero [8–11]. This phase condition is needed because of symmetry conservation, namely, that the initial experimental signal has no phase difference across the dark region, and the zero phase change property should be conserved, as analyzed in detail in Ref. [9]. Experimentally, the formation of such a dark soliton pair from a single dark input signal has been observed not only for temporal solitons in optical fibers [12,13] but also for spatial optical solitons in Kerr-like media [14], photovoltaic media [15], and photorefractive crystals [7], but the phase signature of the dark soliton pairs, namely, *opposite phase jumps*, needs to be demonstrated.

This paper reports experimental evidence for opposite phase jumps of dark soliton pairs. As in Ref. [6], the experiments were carried out with a YIG film strip in a surface spin-wave configuration [16,17] and used as an input signal a single black spin-wave pulse with no phase change. A pair of black solitons with opposite π phase jumps was observed in certain input power and input pulse width ranges. Beyond those ranges, one also observed pairs of gray solitons that showed opposite phase jumps and an overall phase change of zero. The formation of a single black soliton from a dark pulse, similar to that reported previously in Ref. [6], was also observed, but only for an initial black pulse that was very narrow. The experimental results were supported by numerical simulations that made use of the complex Ginzburg-Landau equation [18,19] and the experimental parameters.

Figure 1(a) shows a schematic diagram of the experimental setup. The core components include a long and narrow YIG thin film strip and two microstrip line transducers placed on the top of the YIG strip for the excitation and detection of spin waves. The YIG film strip is magnetized to saturation by an external magnetic field that is in the plane and perpendicular to the length of the YIG film strip. This film-field configuration supports the propagation of surface spin waves [16,17] that show a repulsive nonlinearity [5,20]. The microwave switch is fed by a continuous microwave source and is controlled by a fast pulse generator. It generates black microwave pulses for the excitation transducer. The signals from the detection transducer are analyzed directly by a fast oscilloscope and a spectrum analyzer, without using any microwave amplifiers or diodes.

For the experimental data presented below, the YIG film strip was 5.6 μm thick, 2 mm wide, and 50 mm long. It was cut from a larger single-crystal YIG wafer grown on a gadolinium gallium garnet substrate by liquid phase epitaxy. The magnetic field was set to 909 Oe. The microstrip line transducers were 50 μm wide and 2 mm long and were end shorted. The separation of the two transducers was set to 6.8 mm. The input pulses applied to the excitation transducer were squarelike dips on a continuous microwave signal, with the amplitude at the dips less than 5% of the amplitude of the microwave background. The power level of the microwave

*Corresponding author: mwu@colostate.edu

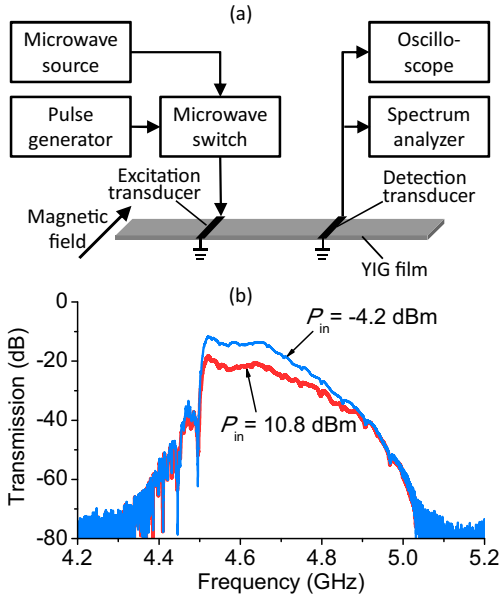

FIG. 1. (Color online) (a) Schematic of the experimental configuration. (b) Transmission responses of the transducer-YIG-transducer structure measured at two different input power levels (P_{in}), as indicated.

background was controlled by a microwave amplifier and a tunable microwave attenuator inserted between the microwave switch and the excitation transducer. The amplifier had a 30 dB dynamic range, a peak output power of 2 W, and a linear

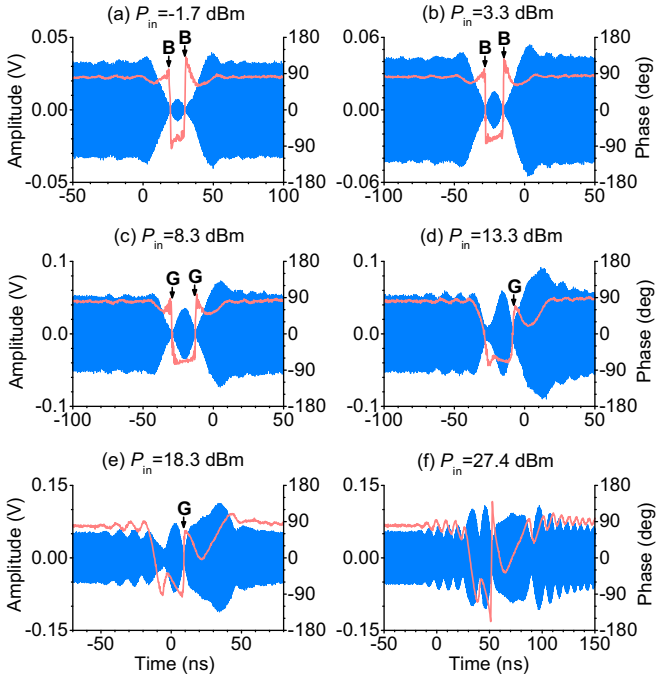

FIG. 2. (Color online) Output signals obtained for a fixed input pulse width of 29 ns and different input power levels (P_{in}), as indicated. The voltage wave signals are shown in light blue, while the wave phase profiles are shown in light red. The black and gray solitons are marked by B and G, respectively.

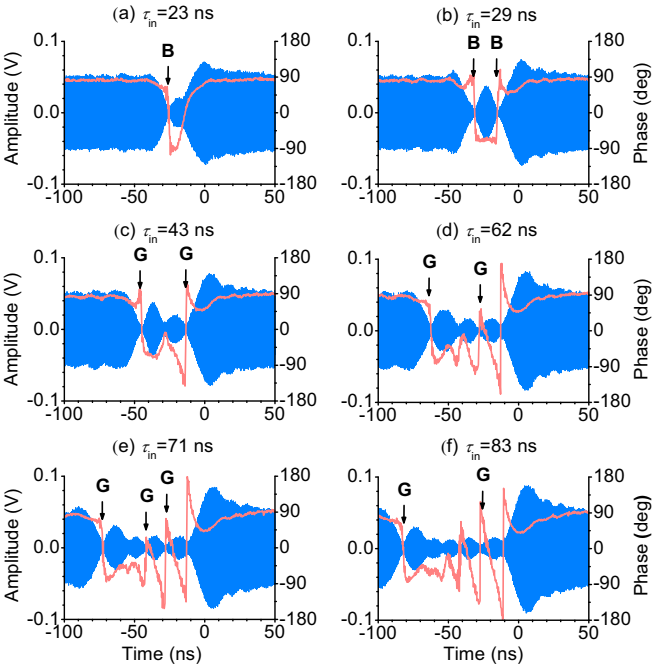

FIG. 3. (Color online) Output signals obtained for a fixed input power of 8.3 dBm and different input pulse widths (τ_{in}), as indicated. The voltage wave signals are shown in light blue, while the wave phase profiles are shown in light red. The black and gray solitons are marked by B and G, respectively.

response from 2 to 8 GHz. These characteristics ensured that the nonlinear response of the system was determined solely by the YIG film.

Figure 1(b) shows the transmission responses (S_{21}) of the transducer/YIG/transducer structure measured at two different input power levels (P_{in}), as indicated. One can see three results from the data in Fig. 1(b): (1) The spin-wave frequency range is about 4.5–5.0 GHz. For the data presented below, the carrier wave frequencies of the input signals all fell within this frequency range. (2) The transmission profiles are relatively smooth. This indicates that the spins on the film surfaces are unpinned, and a repulsive nonlinearity is expected for the entire 4.5–5.0 GHz frequency range. In films with strongly pinned surface spins, one has a repulsive nonlinearity only in narrow frequency ranges [21,22]. (3) The transmission for $P_{in} = 10.8$ dBm is notably smaller than that for $P_{in} = -4.2$ dBm. This difference results from nonlinear damping [23], which was considered in the numerical simulations presented below.

Figures 2 and 3 present representative experimental data for the formation of dark solitons. Figure 2 shows the output signals measured for a fixed input black pulse width $\tau_{in} = 29$ ns and different P_{in} levels, as indicated. Here, P_{in} denotes the power level of the microwave background of the signals applied to the excitation transducer. In contrast to Fig. 2, Fig. 3 shows the output signals obtained for a fixed input power $P_{in} = 8.3$ dBm and different pulse widths, as indicated. In both the figures, the voltage waves are shown in light blue, while the corresponding phase profiles are shown in light red. The black and gray solitons are marked with "B" and "G," respectively. Note that all the data were obtained with an input carrier wave frequency of 4.609 GHz, and the phase profiles show the phase data of the output signals relative to the phase

of a reference continuous wave with the same frequency as the input carrier waves [24].

The data in Figs. 2(a) and 2(b) show the key results of this paper—the demonstration of a pair of black solitons. For each soliton, the dip almost goes to zero, and the phase shows a π jump at its center. For each pair, the phase jumps of the two solitons are opposite, and the overall phase change is zero. With an increase in $P_{\rm in}$, from 3.3 to 8.3 dBm, the black soliton pair evolves into a pair of gray solitons, as shown in Fig. 2(c). For each gray soliton, the dip amplitude is nonzero, and the phase jump is less than π (about 0.92π). Nevertheless, the two solitons have opposite phase jumps, and the total phase change is almost zero, the same as the black soliton pairs in Figs. 2(a) and 2(b). When $P_{\rm in}$ is increased to 13.3 dBm and then to 18.3 dBm, one observes only a single gray soliton, as shown in Figs. 2(d) and 2(e). With a further increase in $P_{\rm in}$, one observes nonsolitonic wave forms only, as shown in Fig. 2(f). Note that independent of the value of $P_{\rm in}$, the zero phase change condition is always satisfied.

The data in Fig. 3 show that the formation of dark soliton pairs also depends on the width of the initial black pulse. Figure 3(b) shows a pair of black solitons obtained at $\tau_{\rm in} = 29$ ns. It is essentially the same as the pairs shown in Figs. 2(a) and 2(b). For a narrower initial black pulse with $\tau_{\rm in} = 23$ ns, however, one observes only a single black soliton, as shown in Fig. 3(a). As will be discussed shortly, this single black soliton is similar to the one reported previously in Ref. [6]. In contrast, for broader initial pulses, one observes multiple gray solitons or nonsolitonic dips, as shown in Figs. 3(c)–3(f). At $\tau_{\rm in} = 71$ ns, for example, the signal consists of three gray solitons and two nonsolitonic dips, as shown in Fig. 3(e). Note that the overall phase change is always zero for all the data shown in Fig. 3, the same as for data in Fig. 2.

The experimental results presented above can be reproduced by numerical simulations using the so-called complex Ginzburg-Landau equation [18,19]

$$i\left[\frac{\partial u}{\partial t} + v_g\frac{\partial u}{\partial x} + \eta u\right] - \frac{1}{2}D_2\frac{\partial^2 u}{\partial x^2} - \frac{1}{6}D_3\frac{\partial^3 u}{\partial x^3} + (N + i\nu)|u|^2 u = 0, \quad (1)$$

where u is the spin-wave amplitude, x is the spatial coordinate, t is the temporal coordinate, v_g is the group velocity, η is the damping coefficient, D_2 is the dispersion coefficient, D_3 is the third-order dispersion coefficient, N is the nonlinearity coefficient, and ν is the nonlinear damping coefficient. In comparison with the standard nonlinear Schrödinger equation [3], Eq. (1) incorporates three additional terms: one describes the third-order dispersion, and the other two describe the linear and nonlinear damping of the spin waves. These additional terms are required in order to reproduce the experimental responses.

The simulations used the split-step method to solve the derivative terms with respect to x and used the Runge-Kutta method to solve the equation with the rest of the terms [25,26]. The split-step method uses Fourier transformation to convert the space domain (x) of the equation into the wave-number domain (k), turning the differential parts of the equation into simpler linear algebra. A high-order Gaussian-type dip, instead of a square black pulse, was used in simulations as the initial black pulse. The use of a square black pulse as an initial pulse gave rise to numerical noise due to the discontinuities at the pulse edges. Though it is also possible to use the fundamental Gaussian function, a high-order Gaussian dip better resembles the experimental situation.

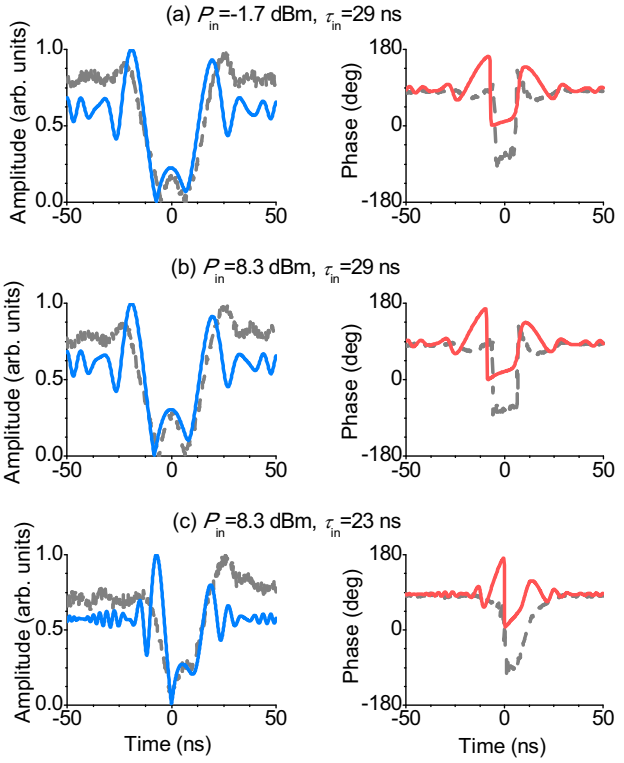

FIG. 4. (Color online) Comparisons between experimental data and numerical simulations. The gray dashed curves show the data measured at different input power or input pulse widths, as indicated. The light blue and light red curves show the simulated envelope and phase profiles, respectively. The simulations shown in (a), (b), and (c) were obtained with $u_{\rm in} = 7\times10^{-5}$ and $\tau_{\rm in} = 29$ ns, $u_{\rm in} = 8\times10^{-4}$ and $\tau_{\rm in} = 29$ ns, and $u_{\rm in} = 8\times10^{-4}$ and $\tau_{\rm in} = 23$ ns, respectively. For easy comparison, all the profiles were normalized in amplitude and shifted in time.

Figure 4 shows representative simulation results. In each row, the gray dashed curves show the envelope and phase profiles of the signal measured at certain $P_{\rm in}$ and $\tau_{\rm in}$ values, as indicated, while the light blue and light red curves show the simulated envelope and phase profiles, respectively. The simulations presented in Figs. 4(a)–4(c) were carried out with $u_{\rm in} = 7\times10^{-5}$ and $\tau_{\rm in} = 29$ ns, $u_{\rm in} = 8\times10^{-4}$ and $\tau_{\rm in} = 29$ ns, and $u_{\rm in} = 8\times10^{-4}$ and $\tau_{\rm in} = 23$ ns, respectively, where $u_{\rm in}$ denotes the background amplitude of the initial spin-wave signal. The other parameters used are as follows: $v_g = 3.6\times10^6$ cm/s, $\eta = 5.28\times10^6$ rad/s, $D_2 = -3\times10^3$ rad $\cdot$ cm^2/s, $D_3 = 1$ rad $\cdot$ cm^3/s, $N = -1\times10^{10}$ rad/s, and $\nu = 6.28\times10^9$ rad/s. Among these parameters, $u_{\rm in}$ is the only fitting parameter, while all others were calculated based on the properties of the YIG film sample. Note that the experimental and numerical results in Fig. 4 are normalized in amplitude and shifted in time for the purpose of easy comparison.

One can see from the data in Fig. 4 that the experimental responses can be well reproduced by numerical simulations.

Furthermore, the simulations presented in Fig. 4, together with additional simulations, indicate two important results as follows. First, a black spin-wave pulse genetically evolves into a pair of black solitons, as in Figs. 2(a), 2(b), and 3(b), or a pair of gray solitons, as in Fig. 2(c), for a certain initial power range and a certain initial pulse width range. All of the soliton pairs show an overall phase change of zero. These results agree with theoretical expectations [8–10]. Second, when the initial black pulse is too narrow to evolve into a soliton pair, it may develop into a single black soliton-like object, as shown in Fig. 4(c). This is similar to that reported previously in Ref. [6] and is consistent with the standard nonlinear Schrödinger equation model [3,5]. The existence of a single black soliton, however, does not break the zero phase change condition. This is clearly shown by the two phase profiles shown in Fig. 4(c). The simulated profile shows a phase jump of $-\pi$ at the soliton center, a gradual increase in the phase for the wave forms both leading and following the soliton, and an overall phase change of zero. The experimental profile shows a slightly different feature—the phase undergoes a jump of $-\pi$ at the soliton's center and a gradual phase increase of π for the wave form following the soliton. In addition, the simulations also indicated that the slight asymmetry of the experimental amplitude and phase profiles was associated with the third-order dispersion.

Several important points should be noted. First, in addition to providing experimental evidence for the intrinsic phase characteristic of dark soliton pairs, this paper also demonstrates that dark soliton pairs not only exist in optical systems [7,12–15] but also take place in spin-wave systems, thereby indicating the universal feature of the dark soliton pair phenomenon. Second, previous work on spatial solitons has indicated that an initial dark signal could also develop into a sequence of dark solitons whose number is more than two and is even [7,10]. It is important that future work demonstrate such development for temporal dark solitons and study the phase features of the solitons. Third, the numerical simulations in this paper indicate that the complex Ginzburg-Landau equation [18,19] appears to be a more accurate model for nonlinear spin waves in magnetic thin films than the standard nonlinear Schrödinger equation, although the latter has been proved to be a generally good model for many different types of nonlinear waves [3,5]. Finally, the simulations in this paper revealed the existence of a soliton triplet that consists of a bright soliton embraced by two black solitons. The data in Fig. 2(c) present a similar effect. Future study, both experimental and theoretical, on such soliton triplets is of great interest.

In summary, this paper reported on the formation of black soliton pairs from nonlinear black spin-wave pulses. For each soliton, the dip almost goes to zero and the phase shows a π jump at its center. For each pair, the phase jumps of the two solitons have opposite signs and the overall phase change is zero. The formation of such black soliton pairs requires the initial black pulses to have appropriate power and widths. Beyond them, the formation of a gray soliton pair is also possible, which also shows opposite phase jumps and a zero overall phase change as the black soliton pairs. When the initial pulses are too narrow to support black or gray soliton pairs, they can evolve into single black solitons. This is consistent with the standard nonlinear Schrödinger equation [3,5] and the previous experimental observation [6].

This paper was supported, in part, by the U.S. National Science Foundation (Awards No. DMR-1407962 and No. ECCS-1231598) and the Russian Science Foundation (14-12-01296).

[1] A. Hasegawa and Y. Kodama, *Solitons in Optical Communications* (Oxford University Press, New York, 1995).
[2] Y. S. Kivshar and B. Luther-Davies, Phys. Rep. **298**, 81 (1998).
[3] M. Remoissenet, *Waves Called Solitons: Concepts and Experiments* (Springer-Verlag, Berlin, 1999).
[4] A. N. Slavin, Y. S. Kivshar, E. A. Ostrovskaya, and H. Benner, Phys. Rev. Lett. **82**, 2583 (1999).
[5] C. Sulem and P.-L. Sulem, *Applied Mathematical Sciences* (Springer, New York, 1999), Vol. 139.
[6] M. Chen, M. A. Tsankov, J. M. Nash, and C. E. Patton, Phys. Rev. Lett. **70**, 1707 (1993).
[7] Z. Chen, M. Mitchell, and M. Segev, Opt. Lett. **21**, 716 (1996).
[8] K. J. Blow and N. J. Doran, Phys. Lett. A **107**, 55 (1985).
[9] A. N. Slavin, IEEE Trans. Magn. **31**, 3479 (1995).
[10] Z. Chen, M. Segev, S. R. Singh, T. H. Coskun, and D. N. Christodoulides, J. Opt. Soc. Am. B **14**, 1407 (1997).
[11] Y. H. Zhang, K. Q. Lu, J. B. Guo, K. H. Li, and B. Y. Liu, Eur. Phys. J. D **66**, 65 (2012).
[12] D. Krökel, N. J. Halas, G. Giuliani, and D. Grischkowsky, Phys. Rev. Lett. **60**, 29 (1988).
[13] A. M. Weiner, J. P. Heritage, R. J. Kawkins, R. N. Thurston, E. M. Kirschner, D. E. Leaird, and W. J. Tomlinson, Phys. Rev. Lett. **61**, 2445 (1988).
[14] B. Luther-Davies and X. Yang, Opt. Lett. **17**, 496 (1992).
[15] M. Taya, M. C. Bashaw, M. M. Fejer, M. Segev, and G. C. Valley, Opt. Lett. **21**, 943 (1996).
[16] P. Kabos and V. S. Stalmachov, *Magnetostatic Waves and Their Applications* (Chapman and Hall, London, UK, 1994).
[17] D. D. Stancil and A. Prabhakar, *Spin Waves—Theory and Applications* (Springer, New York, 2009).
[18] A. M. Kosevich, B. A. Ivanov, and A. S. Kovalev, Phys. Rep. **194**, 117 (1990).
[19] I. V. Barashenkov and V. G. Makhankov, Phys. Lett. A **128**, 52 (1988).
[20] M. Wu, in *Solid State Physics*, edited by R. Camley and R. Stamps (Academic Press, Burlington, MA, 2011), Vol. 62, pp. 163–224.
[21] B. A. Kalinikos and A. N. Slavin, J. Phys. C **19**, 7013 (1986).
[22] B. A. Kalinikos, N. G. Kovshikov, and A. N. Slavin, Zh. Eksp. Teor. Fiz. **94**, 159 (1988).
[23] M. M. Scott, C. E. Patton, M. P. Kostylev, and B. A. Kalinikos, J. Appl. Phys. **95**, 6294 (2004).
[24] J. M. Nash, P. Kabos, R. Staudinger, and C. E. Patton, J. Appl. Phys. **83**, 2689 (1998).
[25] J. A. C. Weideman and B. M. Herbst, SIAM J. Numer. Anal. **23**, 485 (1986).
[26] D. Pathria and J. L. Morris, J. Comput. Phys. **87**, 108 (1990).